SECOND TEST OF A HELICOPTER INDIVIDUAL BLADE CONTROL SYSTEM IN THE NASA AMES 40- BY 80-FOOT WIND TUNNEL

Stephen A. Jacklin
NASA Ames Research Center
Moffett Field, California

Achim Blaas
ZF Luftfahrttechnik, GmbH
Kassel-Calden, Germany

Stephen M. Swanson
Sterling Software
Mountain View, CA

Dietrich Teves
Eurocopter Deutschland, GmbH
Munchen, Germany

Abstract

This paper reports the results of a second full-scale wind tunnel test of helicopter individual blade control (IBC) system to improve rotor performance, to reduce blade vortex interaction (BVI) noise, and to alleviate helicopter vibrations. In addition, discussions of the blade and control system loads and IBC hydraulic power requirements are also presented. For this test, the pitch links of the rotor were replaced by servo-actuators to enable the pitch of each blade to be controlled independently of the other blades. The IBC servo-actuators and control system were designed and manufactured by ZF Luftfahrttechnik, GmbH. The wind tunnel test was conducted in the 40- by 80-Foot Wind Tunnel at the NASA Ames Research Center using a BO 105 helicopter rotor. The acquired data set includes data on rotor performance, the static and dynamic hub forces and moments, rotor loads, control system loads, inboard and outboard blade pitch motion, and BVI noise. The data indicated that reductions in BVI noise of up to 12 db and reductions in the dominant 4/rev hub loads could be obtained simultaneously using multi-harmonic IBC input. The data also showed that performance improvements of up to 7 percent could be obtained at high-speed forward flight conditions using 2/rev IBC inputs.

The IBC test program was an international collaborative effort between NASA, the U.S. Army AFDD, ZF Luftfahrttechnik, Eurocopter Deutschland, and the DLR Institute of Flight Mechanics and was conducted under the auspices of the U.S./German Memorandum of Understanding on Helicopter Aeromechanics.

Presented at the American Helicopter Society 2nd International Aeromechanics Specialists' Conference, Bridgeport, CT, October 11-13, 1995.

Notation

BVI	blade vortex interaction
C_T/σ	rotor thrust coefficient
D_{EQ}	equivalent airframe drag area, ft^2
IBC	individual blade control
N	number of blades
n	IBC input harmonic number
n/rev	"n" cycles per rotor revolution
Q	rotor shaft torque, ft-lbs
RTA	NASA/U.S. Army Rotor Test Apparatus
q	dynamic pressure
R	rotor radius, 16.1 ft
Ω	revolution speed, 44.4 rad/sec
Ψ	rotor azimuth angle, deg
α_S	shaft angle, deg
μ	advance ratio
θ_i	pitch of ith blade
σ	rotor solidity, 0.07

Test Hardware and Instrumentation

The IBC tests were performed in the NASA Ames 40- by 80-Foot Wind Tunnel. The test section of this closed-circuit wind tunnel is treated with sound absorptive material to allow near-anechoic acoustic measurements down to 500 Hz. Airspeeds of up to 300 kts may be achieved.

For the IBC testing, a four-bladed, hingeless, BO 105 rotor was mounted to the NASA/U.S. Army Rotor Test Apparatus (Fig. 1). This rotor had a radius of 16.1 ft, a linear blade twist of 8 deg, a solidity of 0.07, and NACA 23012 airfoils. The rotor blades, pitch horns, and hub were standard BO 105 helicopter flight hardware owned by NASA. The IBC actuators replaced the normal BO 105 rotor system pitch links, as shown in Fig. 2. References 21-23 provide a full discussion of the IBC servo-mechanism arrangement, the IBC actuator characteristics, the automatic emergency shutdown features used to maintain system safety, and the computer system used to control the IBC actuators. These references also explain in detail how the RTA was modified for the IBC test to permit the transfer of hydraulic fluid to the IBC actuators in the rotating system.

Table 1 presents a list of the instrumentation placed on the rotor blades, control system, and test stand. Strain gages were used to measure loads on the blades and control system. The IBC motion at the blade tip was calculated from miniature accelerometers located at the blade tip and oriented to measure rotation (Ref. 23). Miniature surface-mounted pressure transducers were used to detect the presence of blade-vortex interactions at four leading edge blade locations.

The RTA static/dynamic rotor balance was used to measure the rotor thrust, side force, drag force, pitching moment and rolling moment. These forces and moments were transformed into forces and moments in the hub plane. Both averaged and time-history loads were measured. The time history data provided information on the vibratory hub loads.

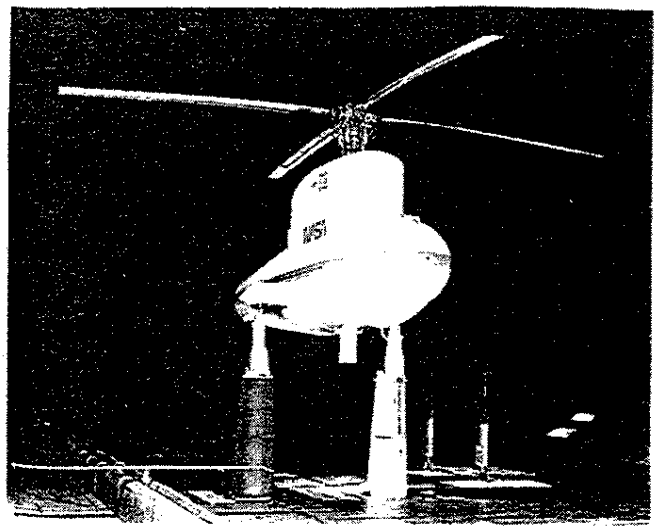

Figure 1. Installation of the RTA and BO 105 rotor in the NASA Ames 40- by 80-Foot Wind Tunnel.

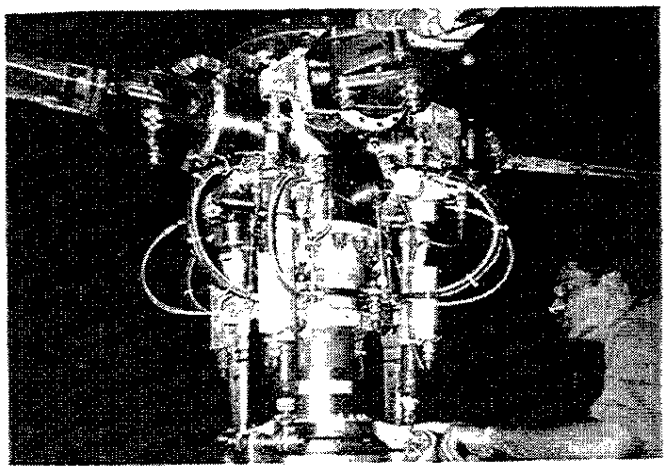

Figure 2. Rotor hub showing placement of IBC actuators.

The rotor shaft flex-coupling was instrumented for shaft torque and the rotor shaft was instrumented with strain gages to measure the mast bending moment.

The displacements and forces of both the stationary swashplate control actuators and the rotating IBC actuators were measured. Each IBC actuator had two LVDTs to provide a dual position measurement. Loads on the control system were evaluated by measuring the axial forces (or pitch link loads) developed in each of the four IBC actuators and each of the three control rods which controlled the

Table 1. Instrumentation.

Measurement	Location and Number
Rotor Blade:	Location, in (R=193.2 in)
Blade Flap Bending	20, 110 in
Blade Chord Bending	28, 110 in
Blade Torsion Moment	65, 77, 110, 155 in
Blade Pressures	116, 135, 155, 174 in
Blade Accelerometers	58, 97, 135 in (flapwise)
Blade Tip Accelerometers	Leading & trailing edges
Rotor Balance:	Lift, side, and drag forces Pitch and roll moments
Rotor Mast:	
Flex-coupling	Shaft torque
Rotor Shaft	Shaft bending moment
Control System:	
IBC Actuator Position	8 (2 per actuator)
IBC Actuator Forces	4 (1 per actuator)
Swashplate Position	3 (1 per control rod)
Swashplate Link Force	3
Rotating Scissors	2
Stationary Scissors	1
Blade Pitch Transducers	4 (1 per blade)
Microphones:	
Stationary	3, retreating side
Traverse	4, advancing side

Introduction

Helicopter control through the conventional swashplate is fundamentally limited for rotor systems having four or more main rotor blades. The three degrees of freedom afforded by the conventional swashplate (1 collective and 2 cyclic) allow the individual pitch control of up to three blades at most. Whereas this shortcoming of the conventional swashplate poses no problems for maintaining helicopter trim in forward flight, it does limit the degrees of freedom available for improving rotor performance, reducing rotorcraft vibrations, and reducing helicopter noise.

Although individual blade control (IBC) has long been proposed as a method for reducing helicopter vibrations and improving helicopter performance [Refs. 1-6], most of the work in this area has centered on active control schemes using actuators in the fixed system. The most prevalent of these methods, the higher harmonic control (HHC) method, was thoroughly tested through analysis, wind tunnel, and flight testing. These investigations have shown that HHC can be used to reduce helicopter vibrations [Refs. 7-14]. It has been shown that HHC can also be used to achieve moderate reductions in helicopter blade-vortex interactional (BVI) noise [Refs. 15-17]. However, the HHC inputs needed to produce the best BVI noise reductions have been found to be different from those needed for good vibration reduction. Individual blade control may offer a solution for this problem.

By having more degrees of freedom than HHC, IBC may be used to achieve simultaneous reduction of both BVI noise and vibration. Although not as straight-forward to implement as HHC, some of the conceptual designs proposed to implement IBC also offer the possibility of reducing the weight of the active control system [Ref. 18]. The difficulty, of course, is that for rotors having four (or more) blades, attainment of individual blade control is possible only through the placement of actuators in the rotating system, one per blade.

Desiring to pursue the realization of individual blade control, ZF Luftfahrttechnik, GmbH, began the development of an IBC system more than a decade ago. Designed to replace the pitch links of the rotor system, the IBC actuators were initially proposed for automatic, in-flight rotor blade tracking adjustment. Nevertheless, this use of actuators in the rotating system, one for each blade, represented a breakthrough in rotor control technology. During the 1980s, the reliability of the IBC system was improved through bench testing and the bandwidth of the actuators was increased to produce controls in the frequency range needed for active helicopter vibration reduction.

In 1990 and 1991, ZF Luftfahrttechnik and Eurocopter Deutschland (ECD) conducted the first flight tests of a prototype IBC system on a BO 105 helicopter. The flight tests indicated that vibration reduction was possible using IBC [Refs. 19 and 20]. However, because the stroke of the actuators was restricted (for safety reasons) to 0.25 deg in 1990 and to 0.49 deg in 1991, a full exploration of the IBC system capability was not possible. In addition, the limited speed of the aircraft precluded the testing of 2/rev IBC to increase rotor performance at high-speed conditions.

In order to explore the full potential of individual blade control, a full-scale wind tunnel test program was proposed using a new IBC system having greater control authority and increased frequency response. The testing was part of an international collaborative effort between NASA, the U.S. Army AFDD, ZF Luftfahrttechnik GmbH, Eurocopter Deutschland GmbH, and the DLR Institute for Flight Mechanics and was conducted under the auspices of the U.S./German MOU on Helicopter Aeromechanics. In addition to testing IBC for its ability to reduce vibration and improve rotor performance, NASA proposed testing the IBC system for its ability to reduce blade vortex interaction (BVI) noise as well. The interested reader is referred to Ref. 21 for a full discussion of the plans and preparations made to support the first wind tunnel test effort, and to Ref. 22 for a complete description of the IBC hardware and control system.

In 1993, the first of two IBC wind tunnel tests was conducted at the NASA Ames 40- by 80-Foot Wind Tunnel. Single-frequency, multi-frequency, wavelet, and pulse type IBC inputs were studied. This test clearly indicated that IBC could be used to suppress all vibratory hub shears and moments by up to 70 percent at the transition speed $\mu = 0.1$ [Ref. 23]. A 7 db reduction in BVI noise was also observed at a descent flight condition showing high BVI noise levels ($\mu = 0.15$) [Ref. 24]. These results were very encouraging. However, the test program could not evaluate the capability of IBC to improve rotor performance at high-speed because of a limitation in the Ames Rotor Test Apparatus (RTA) primary control system. A second shortcoming was that multi-harmonic IBC inputs to achieve simultaneous noise and vibration reduction were not evaluated at the same test condition.

To achieve these objectives, a second IBC test was conducted in 1994 after the RTA primary control system had been strengthened. The increase in load carrying capability, however, was not beyond the strength limits of the standard BO 105 helicopter pitch horn, blades, and hub flight hardware. Open-loop IBC inputs were evaluated at flight conditions ranging from low-speed descent flight to forward flight speeds of up to 190 kts ($\mu = 0.45$). The IBC inputs consisted of single-frequency inputs from 2/rev to 6/rev and various multi-harmonic combinations at amplitudes up to 2.5 deg, where "2/rev IBC" denotes a sinusoidal blade pitch input at a frequency of 2 cycles per rotor revolution.

Scope of the Paper

The effect of IBC on BVI noise, 4/rev vibratory hub loads, and rotor performance observed in the second IBC test were previously reported in Refs. 25 & 26. However, the effect of IBC on the blade and control system loads was not presented, nor was there any discussion of the IBC power requirements. These new aspects will be discussed in this paper, after a description of the IBC test hardware and a review of the most significant findings reported in Ref. 25.

Test Hardware and Instrumentation

The IBC tests were performed in the NASA Ames 40- by 80-Foot Wind Tunnel. The test section of this closed-circuit wind tunnel is treated with sound absorptive material to allow near-anechoic acoustic measurements down to 500 Hz. Airspeeds of up to 300 kts may be achieved.

For the IBC testing, a four-bladed, hingeless, BO 105 rotor was mounted to the NASA/U.S. Army Rotor Test Apparatus (Fig. 1). This rotor had a radius of 16.1 ft, a linear blade twist of 8 deg, a solidity of 0.07, and NACA 23012 airfoils. The rotor blades, pitch horns, and hub were standard BO 105 helicopter flight hardware owned by NASA. The IBC actuators replaced the normal BO 105 rotor system pitch links, as shown in Fig. 2. References 21-23 provide a full discussion of the IBC servo-mechanism arrangement, the IBC actuator characteristics, the automatic emergency shutdown features used to maintain system safety, and the computer system used to control the IBC actuators. These references also explain in detail how the RTA was modified for the IBC test to permit the transfer of hydraulic fluid to the IBC actuators in the rotating system.

Table 1 presents a list of the instrumentation placed on the rotor blades, control system, and test stand. Strain gages were used to measure loads on the blades and control system. The IBC motion at the blade tip was calculated from miniature accelerometers located at the blade tip and oriented to measure rotation (Ref. 23). Miniature surface-mounted pressure transducers were used to detect the presence of blade-vortex interactions at four leading edge blade locations.

The RTA static/dynamic rotor balance was used to measure the rotor thrust, side force, drag force, pitching moment and rolling moment. These forces and moments were transformed into forces and moments in the hub plane. Both averaged and time-history loads were measured. The time history data provided information on the vibratory hub loads.

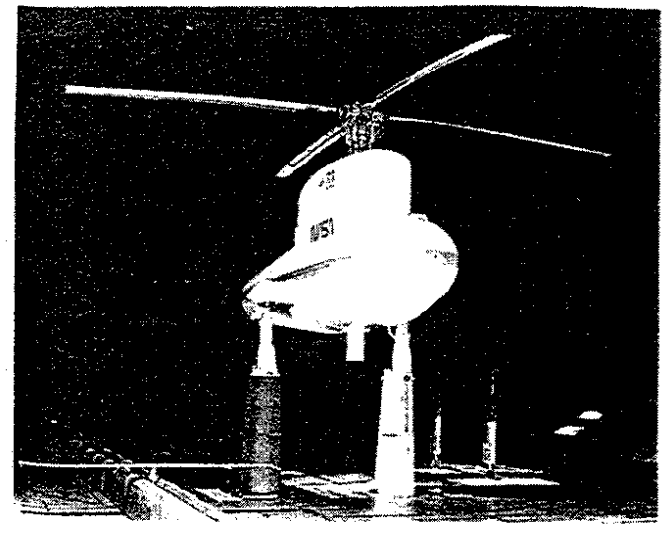

Figure 1. Installation of the RTA and BO 105 rotor in the NASA Ames 40- by 80-Foot Wind Tunnel.

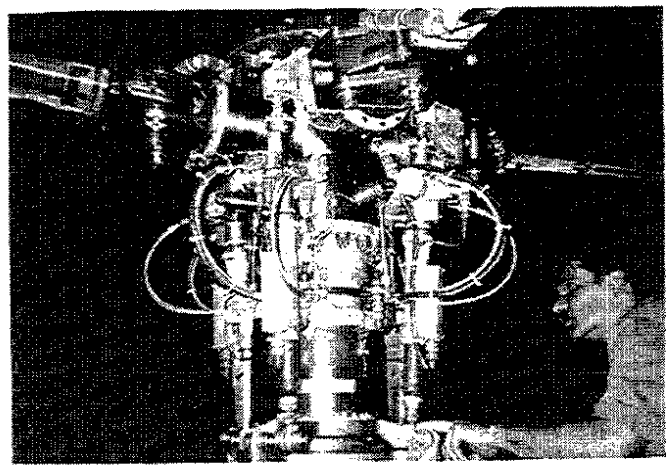

Figure 2. Rotor hub showing placement of IBC actuators.

The rotor shaft flex-coupling was instrumented for shaft torque and the rotor shaft was instrumented with strain gages to measure the mast bending moment.

The displacements and forces of both the stationary swashplate control actuators and the rotating IBC actuators were measured. Each IBC actuator had two LVDTs to provide a dual position measurement. Loads on the control system were evaluated by measuring the axial forces (or pitch link loads) developed in each of the four IBC actuators and each of the three control rods which controlled the

Table 1. Instrumentation.

Measurement	Location and Number
Rotor Blade:	Location, in (R=193.2 in)
Blade Flap Bending	20, 110 in
Blade Chord Bending	28, 110 in
Blade Torsion Moment	65, 77, 110, 155 in
Blade Pressures	116, 135, 155, 174 in
Blade Accelerometers	58, 97, 135 in (flapwise)
Blade Tip Accelerometers	Leading & trailing edges
Rotor Balance:	Lift, side, and drag forces Pitch and roll moments
Rotor Mast:	
Flex-coupling	Shaft torque
Rotor Shaft	Shaft bending moment
Control System:	
IBC Actuator Position	8 (2 per actuator)
IBC Actuator Forces	4 (1 per actuator)
Swashplate Position	3 (1 per control rod)
Swashplate Link Force	3
Rotating Scissors	2
Stationary Scissors	1
Blade Pitch Transducers	4 (1 per blade)
Microphones:	
Stationary	3, retreating side
Traverse	4, advancing side

swashplate attitude in the fixed-system. In addition, the root pitch of each blade was measured using resistive strips at the pitch bearings.

Acoustic data were gathered using a four-microphone traverse system located below the advancing side of the rotor and three fixed microphones located below and aft on the retreating side (Fig. 3 and Table 2). The advancing side microphones were fixed in the lateral and vertical directions and moved by the traverse in the stream-wise direction.

Because data acquisition with the traverse was time-consuming, only a single position of the traverse was used for most data points. To document the directivity effects for IBC inputs producing substantial BVI noise reductions, the traverse was moved streamwise to acquire data at 6 other positions on the advancing side of the rotor.

Definition of IBC Inputs

The IBC pitch input is defined

$$\theta_i = A \cdot Cos\left[n\left(\Psi_1 - (i-1)(90\text{deg})\right) - \phi\right] \qquad (1)$$

where θ_i is the pitch of the ith rotor blade, A is the amplitude, n is the IBC harmonic, Ψ_1 is the rotor azimuth angle of blade No. 1 (measured from 0 deg aft), and ϕ is the

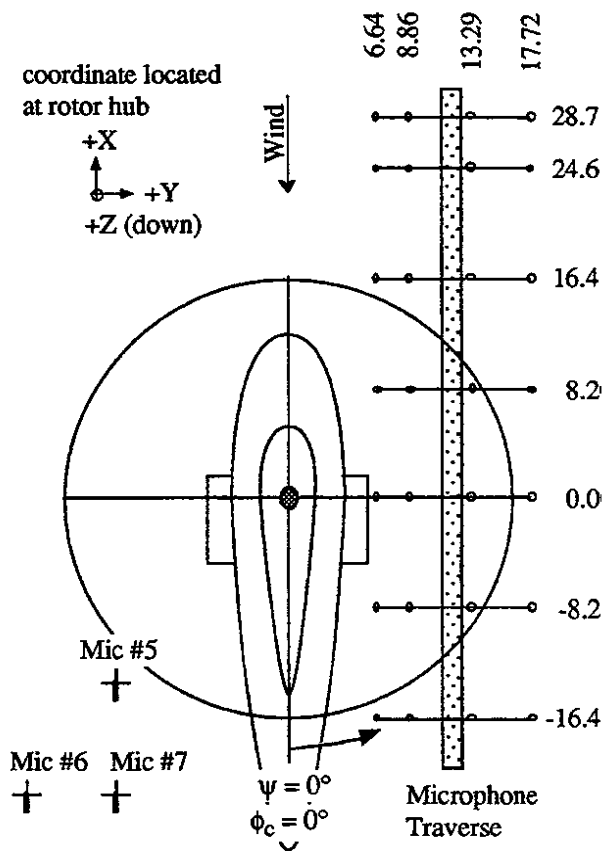

Figure 3. General layout of the microphones relative to the rotor hub center and RTA; all dimensions in feet.

Table 2:

Microphone Positions Relative to the Rotor Hub Center, ft.

	X	Y	Z
Mic 1	*	17.72	18.86
Mic 2	*	13.29	18.86
Mic 3	*	8.86	18.86
Mic 4	*	6.64	18.86
Mic 5	-6.62	-13.29	14.12
Mic 6	-14.62	-13.29	14.12
Mic 7	-14.62	-8.86	14.12

* Variable. See Fig. 3 for the 7 locations.

phase angle of the IBC input. This equation defines the same pitch schedule for each blade relative to its physical azimuth location in the rotor plane. All blades have the same pitch schedule around the azimuth.

To help understand the physics, it is sometimes useful to know the spatial orientation of the IBC input blade pitch. In this paper, ϕ is termed the IBC input phase angle and is used extensively in all of the plots presented herein. It is important to recognize that this phase angle refers to the phase of the control input, not to the rotor azimuth angle, Ψ. For any single-frequency IBC input, the azimuth location of the first maximum blade pitch peak is at rotor azimuth angle of (ϕ/n) deg. The other "n" peaks are located at multiples of (360/n) rotor azimuth angle degs from the first peak. For example, in Fig. 4 the blade pitch added by a 1.0 deg amplitude, 2/rev IBC input at an IBC phase angle of 270 deg is shown. The first peak of this 2/rev "cosine" input has been shifted (270/2) rotor azimuth angle degrees to the right. A second peak follows (360/2) rotor azimuth angle degrees later. Table 3 indicates the location of the first maximum pitch angle as a function of n and ϕ. Obviously, the minima are located halfway between adjacent peaks.

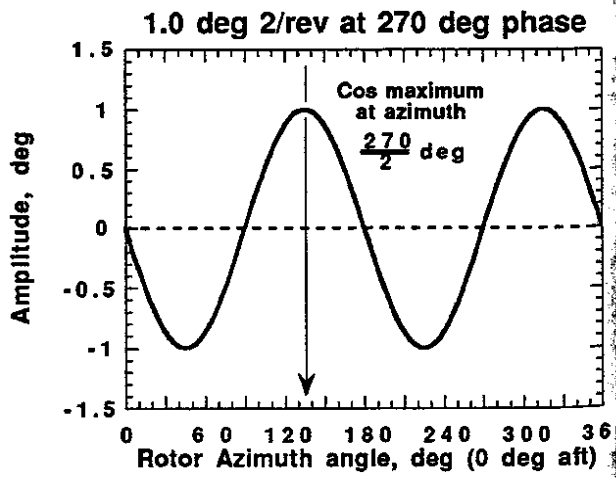

Figure 4: 1.0 deg of 2/rev IBC input at an input phase angle of 270 deg.

Table 3.
Azimuth location of peak IBC pitch input.*

Harmonic (no. peaks)	Spacing Between Peaks	Location of First Peak (Blade Root)	Location of First Peak (Blade Tip)
2/rev	180 deg	ϕ/2 deg	ϕ/2 + 10 deg
3/rev	120 deg	ϕ/3 deg	ϕ/3 + 13 deg
4/rev	90 deg	ϕ/4 deg	ϕ/4 + 33 deg
5/rev	72 deg	ϕ/5 deg	ϕ/5 + 42 deg
6/rev	60 deg	ϕ/6 deg	ϕ/6 + 34 deg

* All locations in degrees of rotor azimuth angle, Ψ.

Two caveats must be remembered when determining the pitch displacement history. First, as explained in Ref. 23, the blade torsional dynamics make the IBC input magnitudes and phases at the blade tip different from those introduced at the blade root. Using the accelerometer data obtained from the blade tip, the approximate phase shifts for each harmonic at the blade tip were calculated and are presented in the last column of Table 3. Second, the 1/rev cyclic trim inputs used to maintain constant hub moment trim were always added to the n/rev IBC inputs. The 1/rev inputs had a considerable effect on the total blade pitch angle, especially for 2/rev and 3/rev IBC inputs. The best understanding of the blade pitch history is gained from the measured blade root pitch angle. The pitch angle at the blade tip can then be found by adjusting the gain and shifting the phase of the IBC input harmonics using the values provided in Ref. 23.

Test Results

Most of the wind tunnel testing was performed at the nominal rotor speed of 425 RPM and the rotor thrust trimmed to 1g ($C_T/\sigma = 0.075$). The IBC data were acquired primarily at the six conditions shown in Table 4. These conditions were: 1) a low-speed forward-flight condition producing high vibration, 2) a descent flight condition having both moderately high BVI noise and vibration, 3) a descent flight condition showing the highest BVI noise, and 4-6) high-speed forward flight conditions for performance improvement studies using 2/rev IBC. A limited amount of vibration control work was also done at condition 4 (127 kts).

In addition to maintaining thrust trim, the 1/rev cyclic control input from the swashplate was adjusted to maintain constant pitch and roll moments for each flight condition. These trim hub moments were estimated from flight test data and are listed in Table 4. Because the hub moments indicated the attitude of the tip-path plane with respect to the shaft, they directly influenced the orientation of the thrust vector with respect to the free stream velocity. Constant moment and thrust trim combined with a fixed shaft angle therefore lead to a constant propulsive force and lift which was needed in order to simulate the rotor in forward flight in the wind tunnel. Therefore, the hub moments and thrust were re-trimmed with each new IBC input in order make sure that the rotor was operating at the same conditions with and without IBC excitation.

Some of the key test results showing the effect of IBC on vibration, BVI noise, and power consumption are presented below.

Vibration Control

Since the RTA was not structurally or dynamically representative of an actual helicopter fuselage, the best characterization of the vibration was obtained through examination of the vibratory forces and moments produced at the rotor hub. These were measured by the RTA rotor balance and then transformed into forces and moments in the hub plane system. Frequency analysis of the hub lift force, side force, drag force, rolling moment, and pitching moment showed that most of the vibratory energy was contained in the fourth harmonic. This, of course, was expected for a 4-bladed rotor since only multiples of the N/rev vibration tend to be transmitted to the fixed system [Ref. 27]. Therefore, in the following discussion, the capability of IBC to alleviate helicopter vibration is explained in the context of controlling the 4/rev vibration component.

The ability of IBC to suppress the vibratory hub loads was tested primarily at condition 1 listed in Table 4 (43 kts, -2.4 deg shaft angle). This condition represented the high vibration found during transition between hover and forward flight. In addition, some testing was also done at condition 4 to evaluate the effects of IBC on vibration at cruise speed.

Table 4. IBC Trim Conditions.

Cond. No.	Adv. Ratio, μ (Speed)	Thrust Coeff. C_T/σ	Shaft Angle α_s	Hub Pitch Moment	Hub Roll Moment	Propulsive Force	Equiv. Des. Velocity
1	.1 (43 kts)	0.075	-2.4 deg	1,400 ft-lb	-300 ft-lb	210 lbs	——
2	.1 (43 kts)	0.075	4.0 deg	1,400 ft-lb	-300 ft-lb	——	446 ft/min*
3	.15 (65 kts)	0.075	2.9 deg	1,600 ft-lb	-350 ft-lb	——	630 ft/min**
4	.3 (127 kts)	0.075	-7.6 deg	1,600 ft-lb	-950 ft-lb	670 lbs	——
5	.4 (169 kts)	0.075	-9.0 deg	1,000 ft-lb	-1,750 ft-lb	780 lbs	——
6	.45 (190 kts)	0.070	-8 deg	1,000 ft-lb	-1,750 ft-lb	640 lbs	——

* Equivalent to 5.87 deg glide slope. ** Equivalent to 5.55 deg glide slope.

The IBC inputs were introduced one harmonic at a time. The amplitude was fixed while the phase of the input was varied. Data was collected at several IBC input phase angles. At the phase angle producing the best vibration reduction (if any), the IBC amplitude was varied.

Although time history data was collected for all of the rotor hub forces and moments, it was expedient to apply the relationships

$$Shear = \sqrt{\left(Side\ Force\right)^2 + \left(Drag\ Force\right)^2}$$
$$Moment = \sqrt{\left(Pitch\ Moment\right)^2 + \left(Roll\ Moment\right)^2} \quad (2)$$

to the 4/rev hub forces and moments. This reduced the vibratory degrees of freedom and allowed better expression of the total vibration reduction achieved. If the moments and forces were not combined, vibratory energy in the pitching moment or side force could be transferred to the rolling moment or drag force, respectively, with no net vibration reduction.

Low-Speed Vibration. The following plots show the effect of IBC on the low-speed vibrations found at the transition speed (43 kts). The vertical axis has units of percent change in the baseline 4/rev vibration. By plotting the percentage of change, presentation of the baseline forces and moments is not required.

Figure 5 presents the effect of 1.0 deg of 2/rev IBC on the hub vibration in forward flight through the transition region. It is seen that the 4/rev forces and moments were best reduced using an input phase angle of about 60 deg. Variation of the input amplitude at this phase, showed that the 4/rev hub shears and moments could be simultaneously reduced by 70-80 percent using 2.5 deg of 2/rev IBC input (Fig. 6). About half the baseline 4/rev lift force (vertical shear force) could be eliminated at the same time. However, where as the shear and moment decreased in proportion to the IBC amplitude up to 2.5 deg, most of the reduction in the vertical shear force was obtained with only 1.5 deg of IBC input.

A phase sweep of 1.0 deg of 3/rev IBC at the same speed, however, showed that the 4/rev vertical shear forces could be almost entirely eliminated using an input phase angle of 150 deg (Fig. 7). Although the 4/rev shear forces and moments were also reduced by 40 percent at that phase angle, they were best reduced at a phase angle of 180 deg. An amplitude sweep at the 150 deg input phase angle showed that a 1.0 deg input amplitude produced the best hub load reductions using 3/rev IBC.

Additional results presented in Ref. 25 show the effect of 4/rev, 5/rev, and 6/rev IBC on low-speed vibration. These results show that 0.5 deg of 4/rev IBC reduced the 4/rev hub shears and moments by 50 % at an input phase angle of 240 deg, while also reducing the vertical lift forces at the same time. While 5/rev and 6/rev IBC could suppress the 4/rev hub shears, hub moments, and hub lift force individually, simultaneous reduction was not possible using these single-

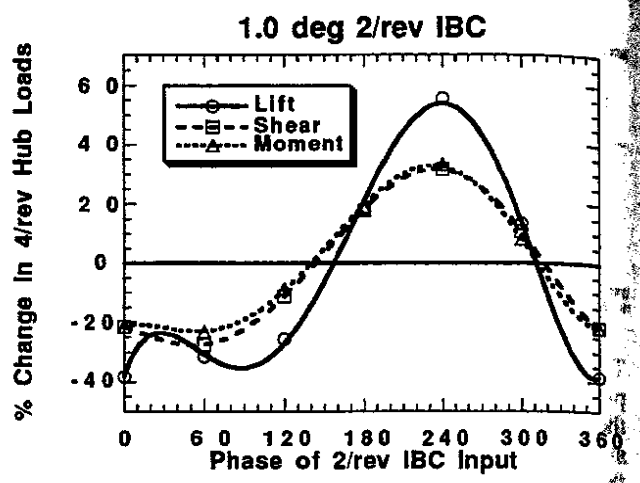

Fig. 5. Phase sweep with 2/rev at 1.0 deg amplitude for 43 kts, α_S= -2.4 deg, C_T/σ = 0.075.

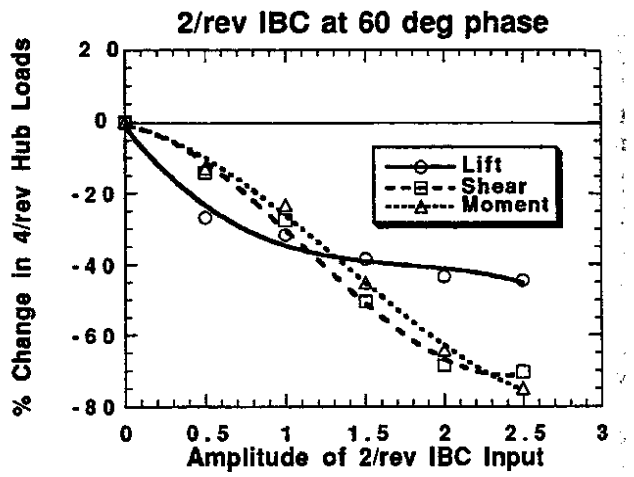

Fig. 6. Amplitude sweep with 2/rev at 60 deg phase for 43 kts, α_S= -2.4 deg, C_T/σ = 0.075.

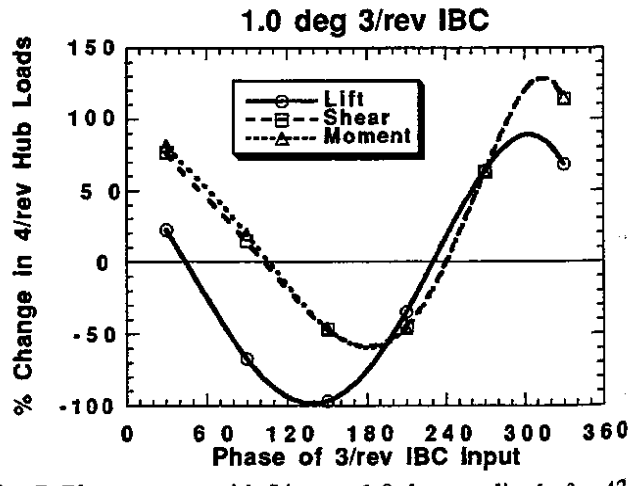

Fig. 7. Phase sweep with 3/rev at 1.0 deg amplitude for 43 kt for α_S= -2.4 deg, C_T/σ = 0.075.

frequency inputs. Therefore, 5/rev and 6/rev IBC were not considered to be very effective inputs for vibration suppression at low-speed.

Cruise Vibration. Only a brief time was spent examining the effects of 2/rev, 3/rev, and 4/rev IBC on the hub oscillatory loads at 127 kts because the overall loads were much less than those found in the transition region. The 3/rev and 4/rev IBC inputs were tested because of their ability to reduce hub loads at low-speed. Testing of 2/rev IBC was also done to judge its effect on rotor performance.

Figures 8 and 9 show the data acquired from application of 2/rev and 3/rev IBC. As can be seen, these inputs generally produced much higher vibration compared to the baseline condition (no IBC). Since it appeared that none of these harmonics were suitable for vibration reduction, no additional data was acquired at the 127 kt condition.

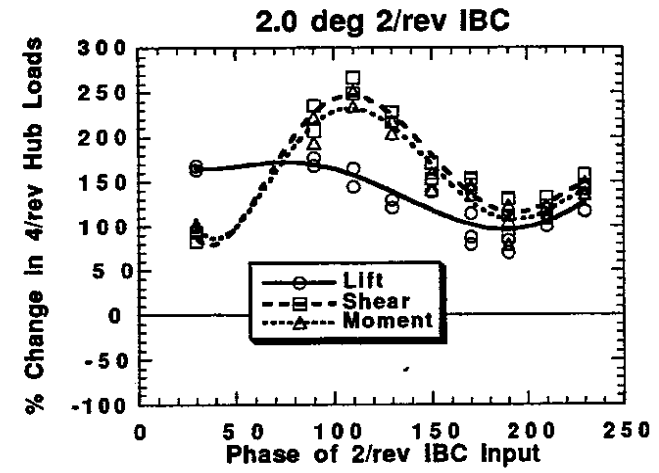

Fig. 8. Percent change in 4/rev hub loads with 2/rev at 2.0 deg amplitude for 127 kts, α_S= -7.6 deg, C_T/σ = 0.075.

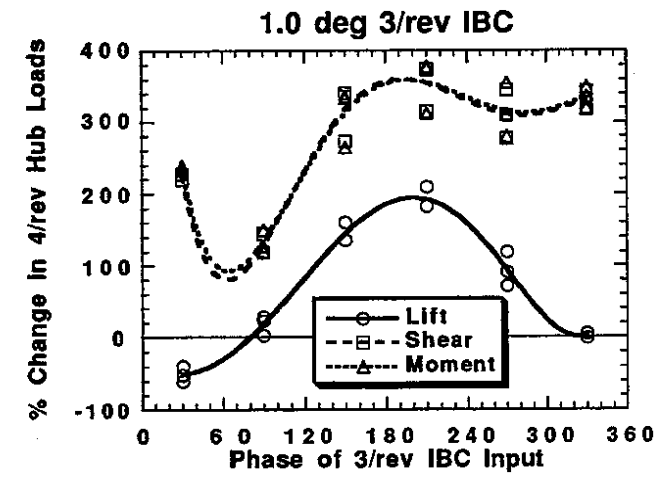

Fig. 9. Percent change in 3/rev at 1.0 deg amplitude for 127 kts, α_S= -7.6 deg, C_T/σ = 0.075.

However, after the wind tunnel test, more insight was gained by plotting the 4/rev sine and 4/rev cosine rotor balance outputs in a two-dimensional graph, similar to a complex number plane. For example, Figs. 10 and 11 show the effect of 2/rev and 3/rev IBC on the 4/rev pitching moments. In these plots, the pitching moments for no IBC input were represented by dots off the origin in each of the plots. If the transference between the IBC inputs and 4/rev pitching moments were perfectly linear, then the oscillatory hub load data would form circles around the baseline (no IBC) points. Nonlinearities would, however, make the hub load plots look more like ellipses.

For the 2/rev IBC input, a very irregular ellipse was formed (Fig. 10). The irregular shape indicated nonlinear behavior, perhaps as the result of couplings to the 1/rev cyclic trim inputs applied to maintain moment trim. The 1/rev cyclic inputs used for this purpose were on the order of 1 deg,

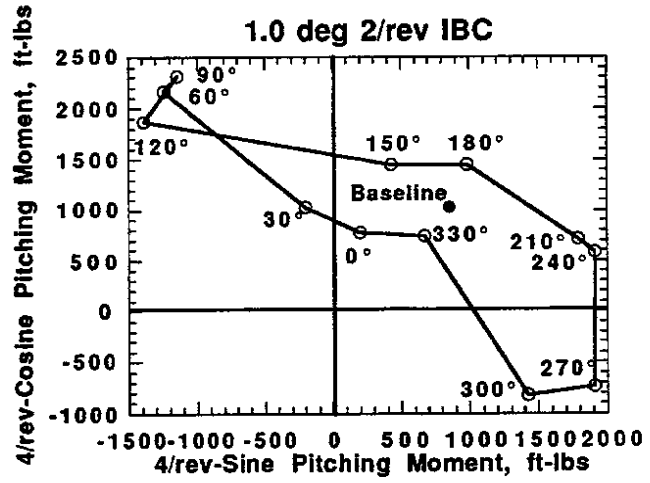

Fig. 10. Polar plot of hub pitching moment for 2/rev IBC at 1.0 deg amplitude for 127 kts, α_S = -7.6 deg, C_T/σ = 0.075.

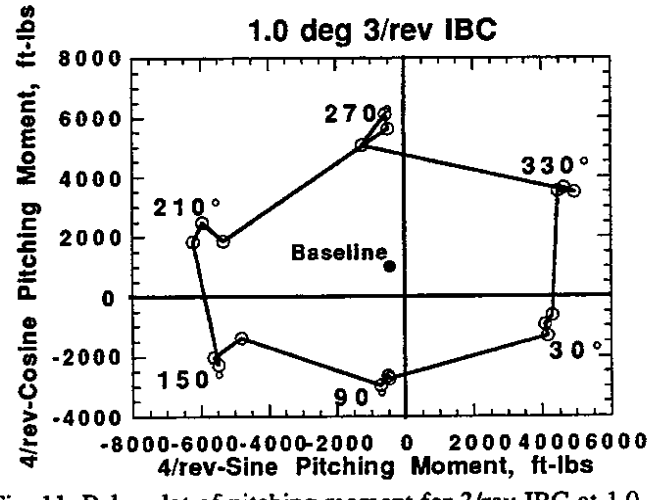

Fig. 11. Polar plot of pitching moment for 3/rev IBC at 1.0 deg amplitude for 127 kts, α_S= -7.6 deg, C_T/σ = 0.075.

depending upon the phase of the 2/rev input. Since the point of zero 4/rev pitching moment (the origin) lay outside the "ellipse", 2/rev amplitudes larger than two degs would probably have been needed to reach it. However, the strong nonlinearity makes it difficult to judge with any certainty.

Making the same plot for the 3/rev IBC inputs, however, resulted in a nearly circular plot (Fig. 11). This indicated a highly linear relationship. Moreover, the required 1/rev cyclic trim adjustments were only on the order of about 0.2 deg, implying much less coupling with the 1/rev trim inputs. Because the zero 4/rev pitching moment origin and baseline were both contained within the ellipse, suppression of the pitching moment vibration at 127 kts could most likely have been achieved using an amplitude much smaller than 1.0 degree. This would have generated a smaller ellipse around the baseline point, which at some input phase angle (approx. 60 deg) would have gone through the zero-4/rev origin.

As shown in Ref. 25, a plot very similar to Fig. 11 could be made using the 4/rev data obtained at 127 kts. Table 5 presents the single harmonic IBC amplitudes thought to be needed for vibration suppression at 43 and 127 kts.

Table 5.
Approximate Single-Frequency IBC Amplitudes Required for Best Vibration Control.

Harmonic	43 kts	127 kts
2/rev	3.0 deg	-----
3/rev	1.0 deg	0.25 deg
4/rev	0.75 deg	0.5 deg
5/rev	0.5 deg	*
6/rev	1.0 deg	*

*Not evaluated

IBC for Simultaneous BVI Noise and Vibration Control

Since the 2/rev, 3/rev, and 4/rev IBC inputs decreased the 4/rev hub moments and forces when applied separately, they were tested for their potential to simultaneously reduce BVI noise and vibration by using a combination of these harmonics. This idea was carefully explored at test conditions having appreciable noise and vibration. At these test conditions, the rotor was tilted backward to simulate typical descent flight conditions producing high BVI noise levels. These trim states are identified as conditions 2 and 3 in Table 4. Both conditions simulated about a 6 deg descent glide slope. Whereas the highest BVI noise levels were produced at the 65 kt airspeed, the highest combined noise and vibration levels were produced at 43 kts using a 4.0 deg shaft angle.

Acoustic data were collected using four microphones on an advancing side traverse and three fixed microphones on the retreating side (Fig. 3). For each microphone, a band-limited sound pressure level was computed as the average energy present in the 150-1500 Hz range, corresponding to the 6th through 40th blade passage frequencies. This frequency band contained nearly all of the BVI noise energy. The reader is referred to Ref. 26 for a complete description of the acoustic data system and acoustic signal processing techniques. In order to save time, traverse sweeps under the advancing side of the rotor were performed to acquire acoustic field data only at the baseline condition (no IBC) and for the points showing the best noise and vibration reductions. Otherwise the traverse was parked at a single location to collect the acoustic data (16.41 ft ahead of the rotor shaft, Fig. 3).

Since the four microphones on the traverse and the three fixed microphones were spaced only a few feet apart, for the purposes of presentation in this paper only, the data from the microphones was averaged using the relationships

$$Adv.BVI = \left(\frac{mic1 + mic2 + mic3 + mic4}{4}\right)$$
$$Ret.BVI = \left(\frac{mic5 + mic6 + mic7}{3}\right) \quad (3)$$

where mic"i" denotes the band-limited BVI noise in db for microphone i. This formed two metrics which could be more easily plotted for the comparison of the advancing and retreating side BVI noise levels. The details of the acoustic field variation with IBC is presented in Ref. 26.

Just as for the vibration cases mentioned in the preceding section, IBC was first applied one harmonic at a time at a fixed amplitude while the phase was varied. Variation of the amplitude was then done at the best phase angle(s) for combined BVI noise and vibration reduction. After the single-frequency inputs were evaluated, some multi-harmonic combinations were also tested.

Single-Frequency IBC Input. Figure 12 shows the effect of applying 1.5 deg of 2/rev IBC at several IBC input phase angles. Both noise and vibration are shown in order to gain an understanding of when both are minimized. The right vertical axis indicates the change in BVI noise (in delta db) and references the advancing and retreating BVI noise metrics plotted as the dashed lines. Also shown in Fig. 12 is an index of the 4/rev hub vibration forces formed

$$Total\ Vibration = Lift + Shear + Moment \quad (4)$$

where the lift, shear, and moment indices refer to the 4/rev vibration content of the lift force and the combined in-plane shear and moment indices of Eq. (2). The relative contributions made by the forces and moments were not weighted in the summation. The left vertical axis in Fig. 12 indicates the percent change in the 4/rev vibration and references the solid curve.

From Fig. 12 it is seen that simultaneous noise and vibration reductions were obtained using 2/rev input phase angles between 0-120 deg, with the best results indicated at a phase angle of 60 deg. Amplitude variation of the 2/rev at

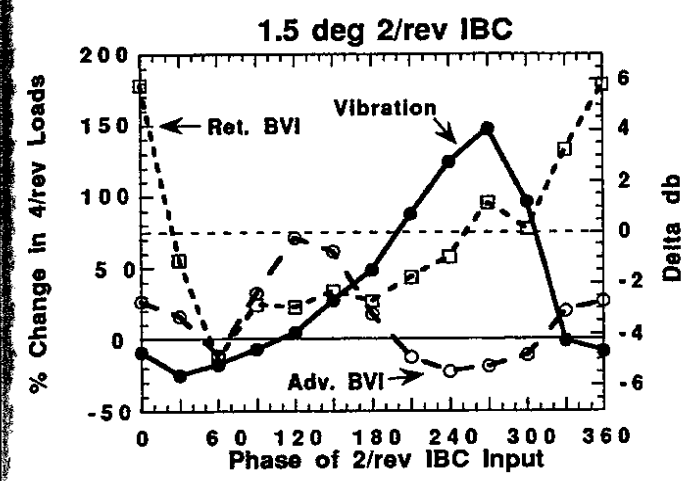

Fig. 12. Vibration and BVI noise reductions with 2/rev IBC at 1.5 deg amplitude for 43 kts, $\alpha = 4.0$ deg, $C_T/\sigma = 0.075$.

60 deg indicated that 1.5-2.0 deg amplitudes yielded the best reductions in BVI noise and vibration. A traverse sweep at this condition indicated that BVI noise reductions of up to 10 db were obtained in front of the rotor on the advancing side, with the average reductions being in the range of about 4-8 db (Fig. 13). The best reduction achieved in 4/rev hub loads was on the order of about 30 percent.

Simultaneous noise and vibration reduction could not be well accomplished using 3/rev IBC. Figure 14 shows that 1.0 deg of 3/rev IBC reduced the advancing side BVI noise at all IBC input phase angles. However the phase angle of lowest vibration (135 deg) maximized the retreating side BVI noise.

In like manner, Fig. 15 shows that 0.5 deg of 4/rev IBC could not simultaneously reduce both noise and vibration. An input amplitude of 1 deg was not used for the phase sweep due to excessive pitch link loads at some phase angles. Simultaneous reduction of advancing and retreating side BVI noise was possible using 4/rev IBC input phase angles between 45 and 180 deg. Unfortunately, at these phase angles the 4/rev vibration level was greatly increased. At 225 deg phase angle, the 4/rev input reduced the vibration by 50 percent and the retreating side BVI noise by an average of 0.5 db, but slightly increased the advancing side BVI noise by an average of 0.5 db.

Single-frequency introduction of 5/rev and 6/rev IBC also showed little promise for simultaneously reducing BVI noise and vibration. As shown in Fig. 16, applied alone, 5/rev IBC always increased the vibration level. Although simultaneous noise and vibration reductions using 6/rev IBC inputs were achieved, the best vibration reduction (60%) was obtained using a phase angle of 240 deg where the retreating side BVI noise was increased (Fig. 17).

Multi-Frequency IBC Input. Having tested all of the single-harmonic IBC inputs, multi-harmonic IBC input was

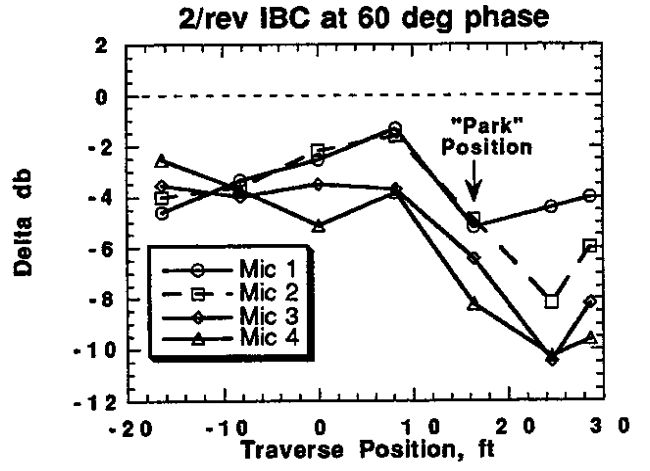

Fig. 13. Traverse sweep with 2/rev IBC at 1.5 deg amplitude and 60 deg phase for 43 kts, $\alpha_S = 4.0$ deg, $C_T/\sigma = 0.075$.

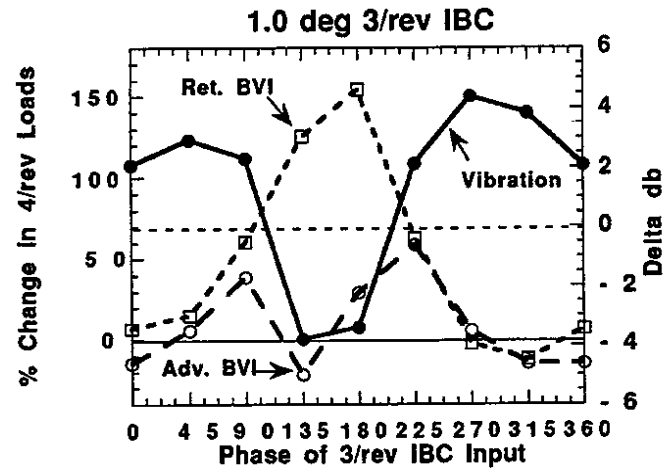

Fig. 14. Vibration and BVI noise reductions with 3/rev IBC at 1.0 deg amplitude for 43 kts, $\alpha_S = 4.0$ deg, $C_T/\sigma = 0.075$.

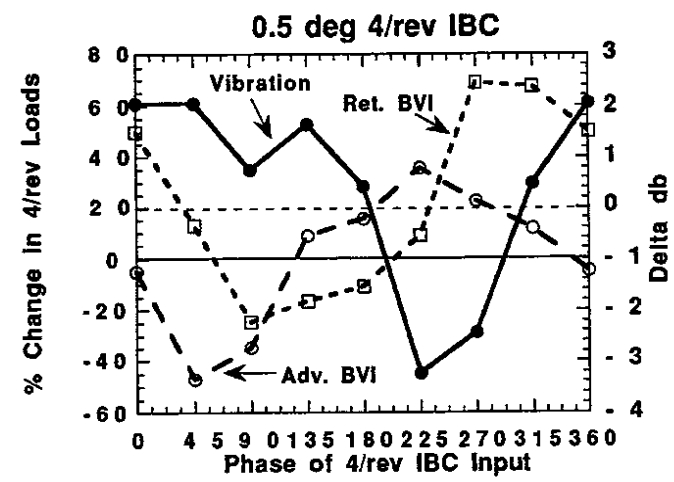

Fig. 15. Vibration and BVI noise reductions with 4/rev IBC at 0.5 deg amplitude for 43 kts, $\alpha_S = 4.0$ deg, $C_T/\sigma = 0.075$.

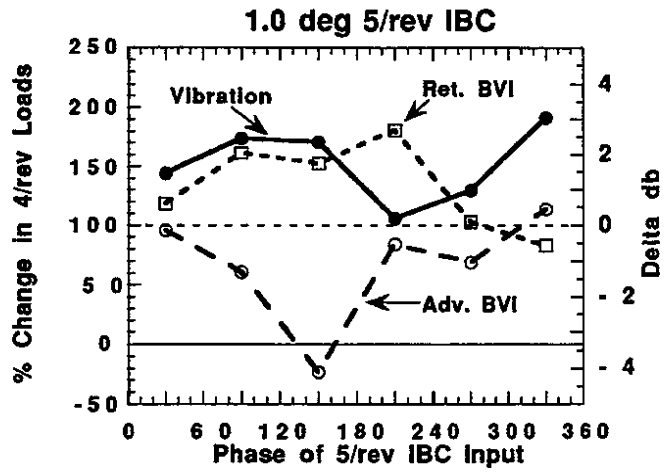

Fig. 16. Vibration and BVI noise reductions with 5/rev IBC at 1.0 deg amplitude for 43 kts, α_S= 4.0 deg, C_T/σ = 0.075.

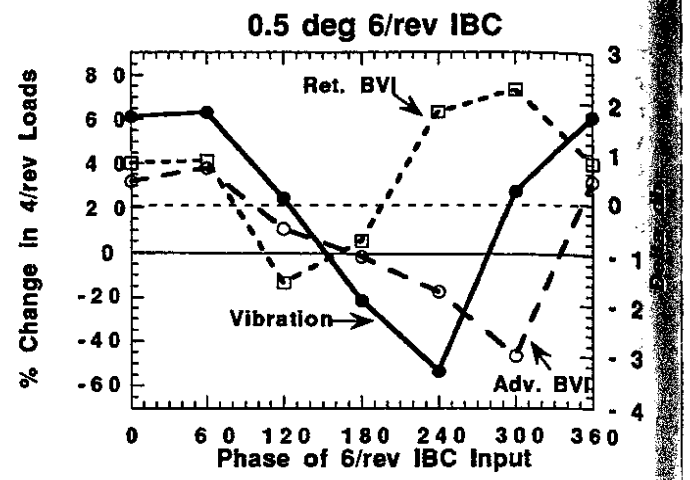

Fig. 17. Vibration and BVI noise reductions with 6/rev IBC at 0.5 deg amplitude for 43 kts, α_S= 4.0 deg, C_T/σ = 0.075.

investigated next. This was more difficult because of the large number of IBC input combinations possible.

Since the best noise reductions were obtained using 2/rev IBC, multi-harmonic IBC combinations were investigated using a 2/rev IBC input held at an amplitude of 1.5 deg and at a phase angle of 60 deg. The other IBC harmonics were then tried in combination with the 2/rev input in the hope of achieving good vibration reductions.

The best simultaneous noise and vibration reductions were obtained using 2/rev and 5/rev. This was despite the fact that 5/rev IBC only increased the hub loads when applied singly (Fig. 16). Figure 18 shows as the phase of a 0.5 deg 5/rev input was varied with the 2/rev input held constant (at 1.5 deg amplitude and 60 deg phase), that at 210 deg phase the 5/rev input simultaneously reduced the advancing side BVI noise by about 7 db, the retreating side BVI noise by 3 db, and the 4/rev vibrations by about 10 percent.

Moreover, an amplitude sweep of the 5/rev input held at 210 deg phase showed that by reducing the amplitude of the 5/rev input to 0.25 deg, the 4/rev vibrations could be suppressed by 85 percent while reducing the advancing side BVI noise by over 10 db (Fig. 19). The retreating side BVI noise was also reduced by over 4 db at the same time. BVI noise reductions of up to 12 db were recorded under the advancing side of rotor at the area of highest measured BVI noise.

Combinations of the other IBC harmonics were tested in the wind tunnel including 2/rev + all others, 2+4+5/rev, 2+4+6/rev, 3+4/rev, and 3+5/rev combinations. Some of these also had the ability to simultaneously suppress BVI noise and vibration. However, none of these combinations were as effective as the 2+5/rev IBC input combination.

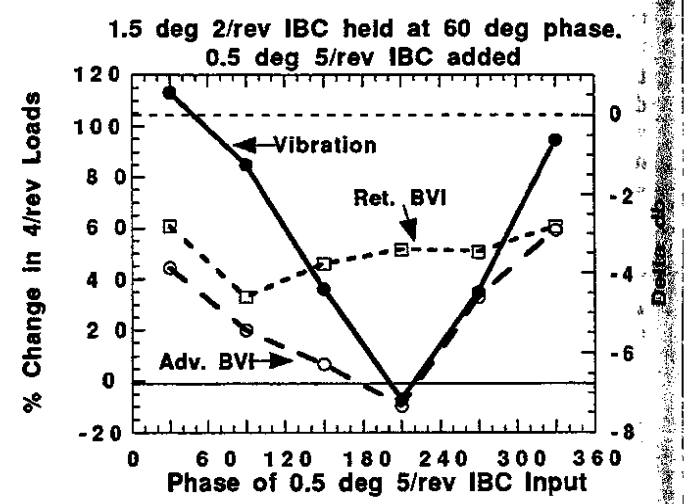

Fig. 18. BVI noise and vibration reduction fixing 2/rev and varying 5/rev phase at 43 kts, α_S= 4.0 deg, C_T/σ = 0.075.

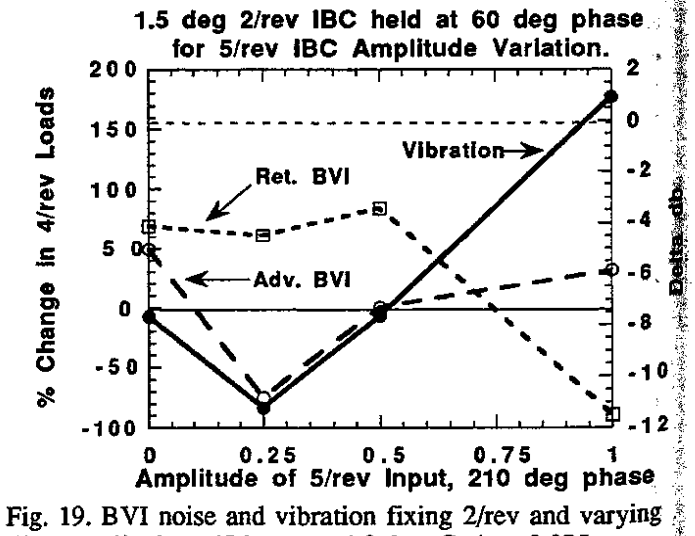

Fig. 19. BVI noise and vibration fixing 2/rev and varying 5/rev amplitude at 43 kts, α_S= 4.0 deg, C_T/σ = 0.075.

IBC for Reduction of Rotor Power Consumption

The ability of 2/rev IBC to reduce the disk loading on the advancing and retreating sides of the rotor in order to help avoid stall and to reduce profile power losses was also evaluated. To maintain thrust equilibrium with 2/rev IBC, the lift must be redistributed from the sides to the front and rear parts of the rotor disk. This task can principally be fulfilled using a 2/rev IBC control input [Refs. 1-6]. Successfully implemented, this form of IBC may reduce the rotor power consumption and extend the flight envelope of the helicopter. Both a reduction of fuel weight and an increase of the flight speed can lead to considerable improvements of the aircraft's productivity [Ref. 28].

The power reductions achievable using 2/rev IBC was evaluated for trim conditions 4-6 of Table 4. For correct evaluation of the performance benefits of IBC, care was taken to keep the propulsive force, thrust, pitching moment, and rolling moment constant during the variation of the 2/rev IBC input. Keeping these quantities constant was very important because they effected the rotor blade angle of attack time history and therefore the induced and profile power contributions. In addition, three data points per IBC input were acquired in order to help reduce the effects of uncertainty in the data caused by any unsteadiness in the test conditions.

At the outset of the test, it was planned to set the rotor thrust at 1g (C_T/σ = 0.075) and the rotor shaft angle a representative propulsive force. Ideally, the proper propulsive force would be that force needed to balance the drag of the aircraft,

$$Thrust \cdot Sin(-\alpha_s) = D_{EQ} \cdot q \qquad (5)$$

where D_{EQ} represents the equivalent airframe drag area (about 10-12 ft^2 for a helicopter of the BO 105 size). Although positive propulsive force was generated at all airspeeds tested, the balance needed to overcome the parasitic drag of the fuselage was only truly simulated at the μ = 0.30 (127 kt) test condition. The full propulsive force could not be developed at the higher airspeeds and shaft angles because the RTA maximum collective pitch control angle was limited to 16 deg to protect the rotor shaft strain gage instrumentation. In addition, the thrust had to be slightly reduced at μ = 0.45 in order to keep the loads below the structural endurance limits. Nevertheless, results were obtained at these conditions.

Figure 20 plots the total power (measured from the rotor torque) versus the phase angle of a 2.0 deg 2/rev IBC input at 127 kts (μ = 0.30). No performance improvement with IBC was obtained. In fact, the 2.0 deg input clearly caused more power consumption at most phase angles. At the worst phase angle, an increase in power consumption of 15 percent was observed.

However, at the 170 kts (μ = 0.40) airspeed, 1.0 deg of 2/rev IBC reduced power consumption by up to 4 percent at input phase angles between 180-200 deg (Fig. 21). Moreover, Fig. 22 shows that by increasing the amplitude of the IBC input, up to 7 percent power reductions were obtained at the best phase angles, with further reductions a possibility given more control authority. This 7% overall reduction in power consumption amounts to about 10% of the rotor profile power.

At an advance ratio 0.45, the IBC control authority was limited to 1.0 deg and the input phase angles between 150 deg and 210 deg in order to keep the rotor loads below the structural endurance limits. It was not possible to obtain a representative propulsive force at this airspeed because of the control system collective limit. Even so, with the shaft angle reduced to -8.0 deg to achieve a representative thrust of C_T/σ = 0.070, between a 5 to 6 percent power reduction was observed (Fig. 23). Had it been possible to perform the testing at the correct propulsive force and nominal 1g thrust settings, larger reductions might have been possible.

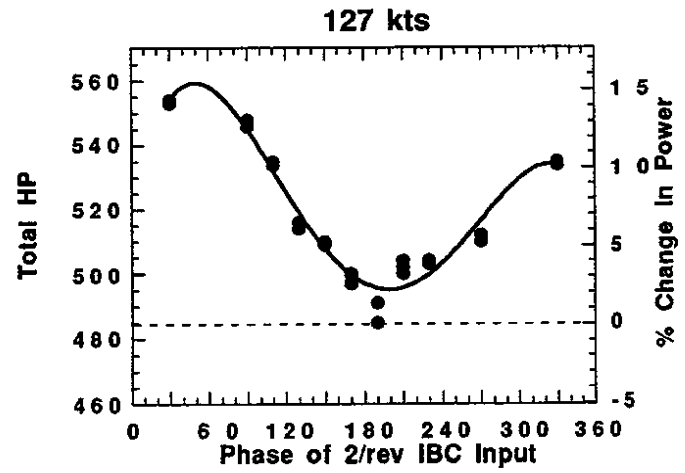

Fig. 20. Total measured shaft horsepower with 2/rev at 2.0 deg amp. for 127 kts, α_S= -7.6 deg, C_T/σ = 0.075.

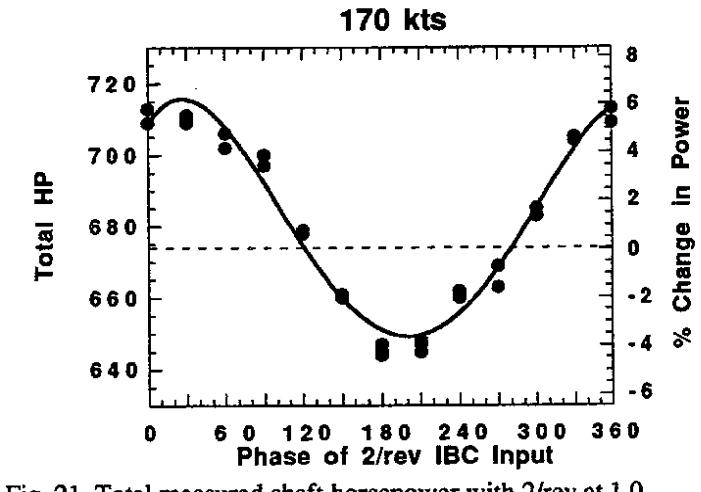

Fig. 21. Total measured shaft horsepower with 2/rev at 1.0 deg amp. for 170 kts, α_S= -9.0 deg, C_T/σ = 0.075.

The mechanism responsible for the power reductions using 2/rev IBC was the creation of a more favorable blade pitch angle of attack around the rotor azimuth. This new angle of attack could have reduced power consumption by avoiding retreating side blade stall or by decreasing the profile power losses on the advancing side of the rotor. In the present wind tunnel test, blade stall was probably not a factor. As shown later in the paper, no major control loads reduction occurred at the phase angles of best power reduction (180-210 deg). Had alleviation of stall been the mechanism responsible for the power savings, a considerable reduction in the pitch link loads would have been expected. This does not mean, however, that 2/rev IBC cannot be used for stall prevention; it simply means that the rotor was probably not operating at a stalled condition in the wind tunnel, even at $\mu = 0.45$.

The theory that the application of 2/rev IBC served to minimize the profile power losses on the advancing side of the rotor seems more plausible. Figure 24 shows a plot of the calculated profile power distribution as a function of the effective angle of attack and the azimuth angle for $\mu = 0.40$ and the radial blade location r/R = 0.9. The calculated baseline angle of attack time history is shown together with the calculated angle of attack time history produced by adding 1.0 deg 2/rev IBC at an input phase of 80 deg. The pitch angle time history at r/R = 0.9 was determined as the sum of the measured blade root pitch angle and the elastic blade deflection calculated from the blade tip accelerometer measurements [Ref. 23]. The profile power distribution shown in Fig. 24 was determined as a function of the effective angle of attack and the azimuth angle by using the two-dimensional airfoil drag coefficient (C_{D2D}) in the manner described in Ref. 29,

$$\frac{\partial P_{Profile}}{\partial r} = f\left(\alpha_{eff}, \Psi\right)$$

$$\frac{\partial P_{Profile}}{\partial r} = \frac{1}{2}\rho \cdot c \cdot C_{D2D}\left(\alpha_{eff}, \mathrm{M}(\Psi)\right) \cdot \Omega^2 R^2 \cdot (S)^{\frac{3}{2}}$$

$$S = \left(\frac{r^2}{R^2} + 2\frac{r}{R}\mu \sin\Psi + \mu^2\right) \qquad (6)$$

where, the effective Mach Number (M), angle of attach (α_{eff}), and yaw angle (Λ) were computed from

$$M = \frac{\Omega R}{a}\left(\frac{r}{R} + \mu \cdot \sin\Psi\right) \qquad \alpha_{eff} = \alpha \cdot \cos\Lambda \quad (7)$$

and

$$\Lambda = \arccos\left(\frac{\frac{r}{R} \cdot \mu \cdot \sin\Psi}{\sqrt{S}}\right)$$

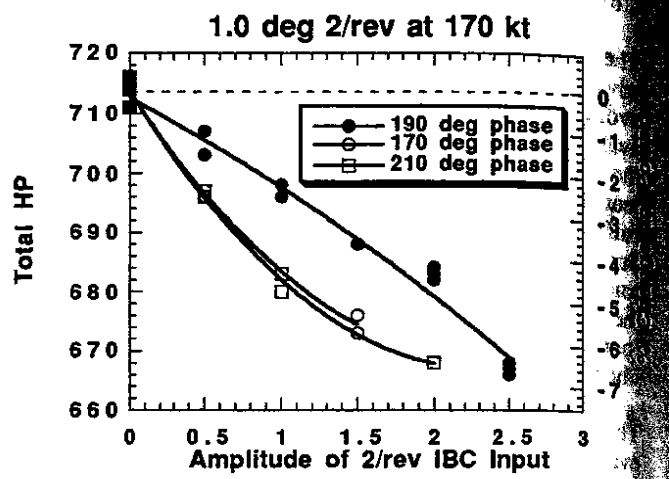

Fig. 22. Total shaft HP with 1.0 deg 2/rev IBC at 170 kt for 170, 190, & 210 deg, α_S= -9.0 deg, C_T/σ = 0.075.

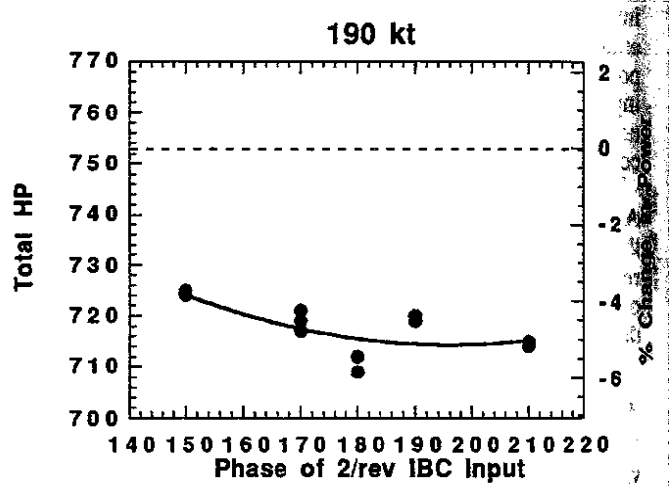

Fig. 23. Total measured shaft horsepower with 2/rev at 1.0 deg amp. for 190 kts, α_S= -8.0 deg, C_T/σ = 0.070.

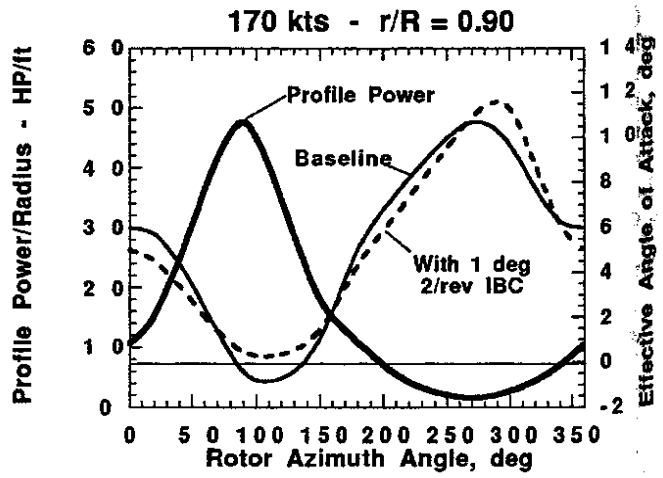

Fig. 24. Calculated profile power and angle of attack for 1.0 deg 2/rev IBC at 170 kt, α_S= -9.0 deg, C_T/σ = 0.075.

omparing the angle of attack time histories shown in Fig. 4, it is seen that the 5 percent power reduction is explained ainly by the reduced rotor blade angle of attack in the first adrant of the rotor azimuth. The elimination of the gative angle of attack at the 90 deg azimuth position, owever, actually produces an increase in the profile power. urther power savings are therefore likely given further timization of the IBC control input in this region.

lthough the reductions in power consumption were smaller an hoped for at the outset of the test, it should be cognized that these small gains are probably sufficient to ff-set any extra weight or drag penalties introduced by the BC system hardware. Moreover, since the rotor could not e operated at a stalled condition in the wind tunnel (due to imitations on the collective input), the ability of 2/rev IBC o reduce retreating blade stall was inadequately investigated. his allows the possibility for considerably higher erformance improvements using 2/rev IBC at other test onditions, including those which more properly simulate he propulsive force at high speed.

ast, with regard to the effect of IBC on power consumption uring the control of BVI noise and vibration (condition 4), t was seen that the additional power consumption was elatively low. Using the most effective BVI noise control armonic, Fig. 25 shows that the power rose 4-6 % as the 2/rev IBC input phase was varied at 1.5 deg amplitude. This ncrease in power consumption can easily be accommodated since the power required for descent flight is half that needed for cruise flight.

Rotor Blade and Control System Loads

Introduction of the IBC inputs placed additional loads on the control system. Figure 26 shows the equivalent pitch link loads measured by the IBC actuator axial force strain gages. The values plotted represent the maximum half peak-to-peak loads encountered for each input. The loads shown are for

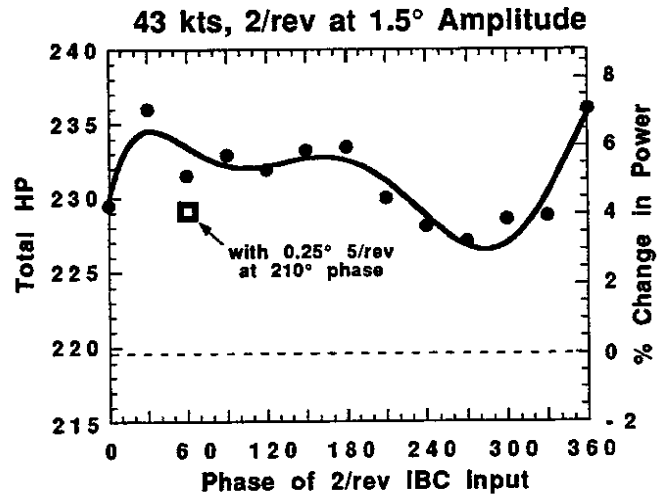

Fig. 25. Total shaft horsepower with 2/rev IBC at 1.5 deg amplitude for 43 kts, α_S= 4.0 deg, C_T/σ = 0.075.

inputs used to reduce BVI noise and oscillatory blade loads in Figs 12-17. As can bee seen, the pitch link loads were increased significantly above the baseline. Normally, pure blade pitch inertial resistance would be expected to increase the pitch link loads proportional to the IBC input amplitude and to the square of the input frequency. However, the relationship shown in Fig. 26 is not that straight-forward. The 2/rev and 6/rev IBC inputs produce the lowest loads because they are reactionless modes. For these input frequencies, the IBC actuators on opposing sides of the swashplate move in phase with each other and provide a better load sharing arrangement. It is noteworthy that the 2/rev pitch link loads were lowest for the IBC inputs that were chiefly responsible for the BVI noise and vibration reductions.

Figure 27 shows that the mid-blade torsional load (r/R = 0.57) followed that of the pitch link loads. The torsional

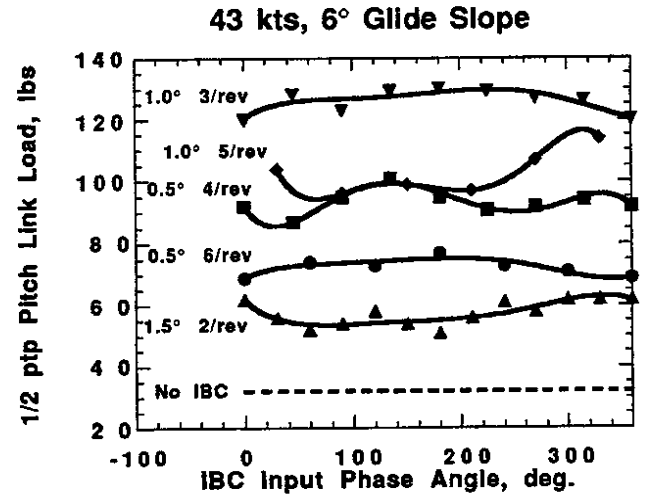

Fig. 26. Pitch link loads with 2/rev - 6/rev IBC input at 43 kts, α_S= 4.0 deg, C_T/σ = 0.075.

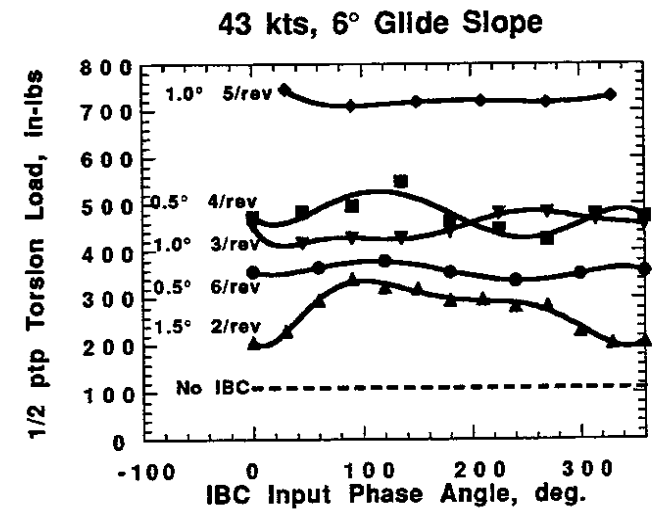

Fig. 27. Effect of IBC inputs on 1/2 ptp torsional bending, Sta. 110, at 43 kts, α_S= 4.0 deg, C_T/σ = 0.075.

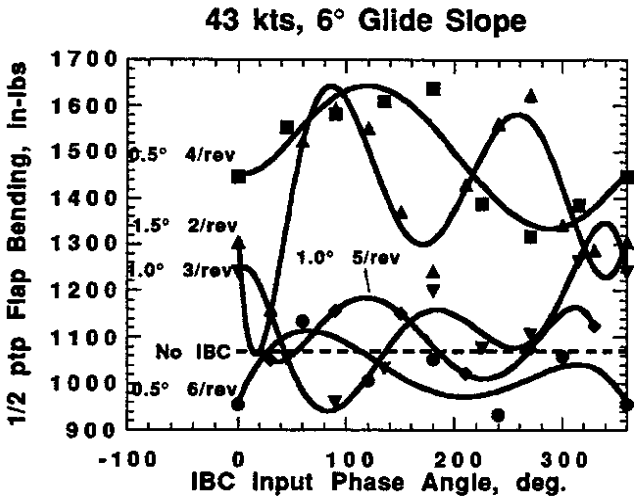

Fig. 28. Effect of IBC inputs on 1/2 ptp flap bending, Sta. 20, at 43 kts, α_S= 4.0 deg, C_T/σ = 0.075.

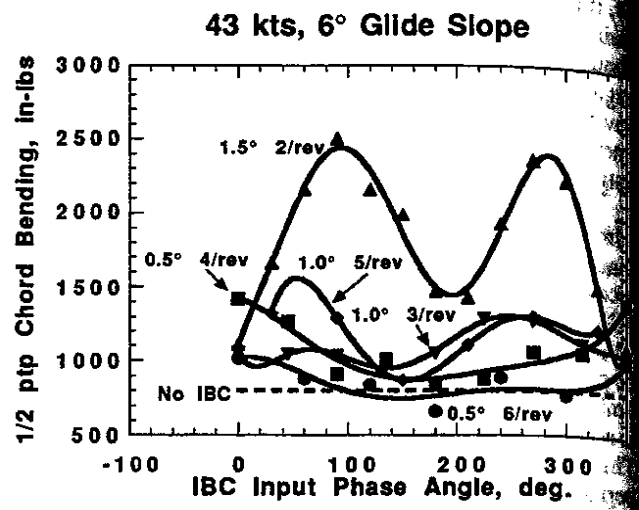

Fig. 29. Effect of IBC inputs on 1/2 ptp chord bending, Sta. 28, at 43 kts, α_S= 4.0 deg, C_T/σ = 0.075.

loads were again significantly higher with IBC. 2/rev and 6/rev input produced the lowest torsional loads.

Interestingly, IBC inputs had different effects on the blade flap bending and chord bending oscillatory loads. As shown in Figs. 28 and 29, the 2/rev input produced large increases in both flap and chord bending. Although the load increases are clearly not trivial, they are below the blade bending endurance limits. Also of interest was that the other IBC harmonics did not increase the blade bending moment as much as they increased the blade pitch link loads. The increase in the bending loads for 2/rev excitation was the result of the input coupling to the blade dynamic response, but this relationship is not clear. Figure 30 shows that at high-airspeeds (trim condition 5), the 2/rev IBC input did not produce great increases in the blade bending loads. The relationship of the IBC inputs to the blade flap and torsion loads deserves further study but is beyond the scope of this report.

Hydraulic Power Requirements for IBC

The IBC actuators required power supplied by the flow of pressurized hydraulic fluid to establish the IBC motions. The power needed to operate the IBC actuators was computed as the product of the hydraulic pressure times the flow rate,

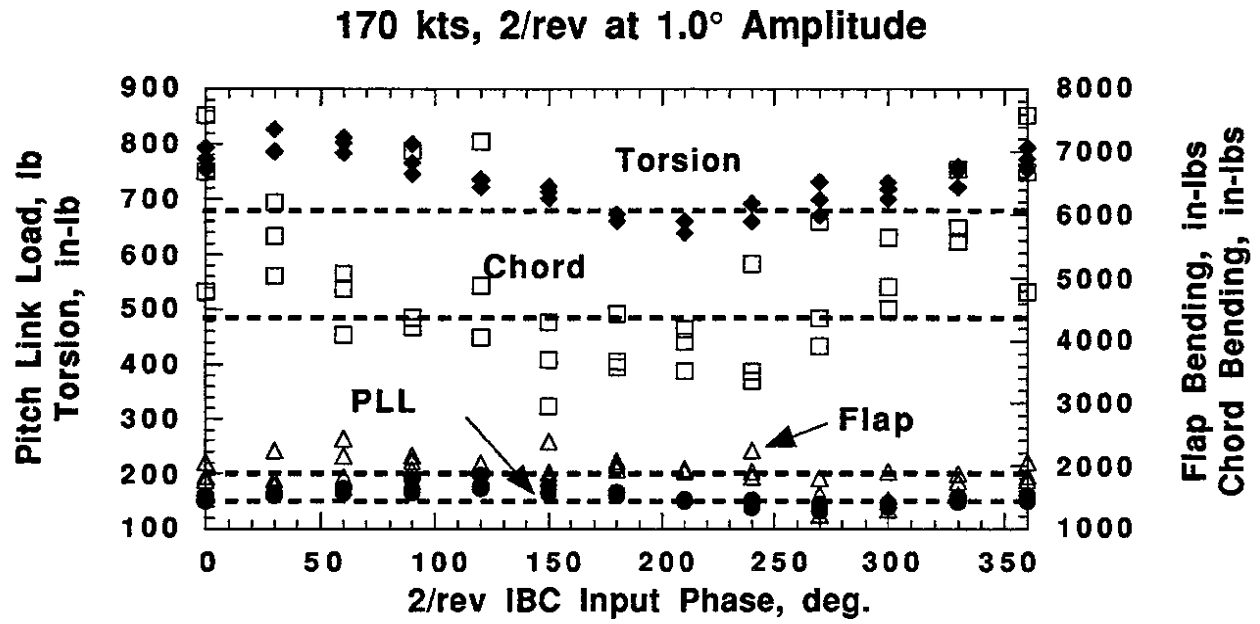

Fig. 30. Phase sweep of 1.0° amplitude 2/rev IBC at 170 kts, α_S= 4.0 deg, C_T/σ = 0.075 showing 1/2 ptp torsional bending, Sta. 110, 1/2 ptp flap bending, Sta. 20, and 1/2 ptp chord bending, Sta. 28.

$$HP = \frac{(PSI \cdot GPM)}{1714} \tag{8}$$

where PSI is the hydraulic pressure in lbs per in^2 and GPM is the flow rate in gallons per minute through the actuator [Ref. 29].

The pressure used in the calculation was not the hydraulic supply pressure of 3000 psi, but rather the pressure developed within the hydraulic cylinder itself. The pressure developed in the hydraulic cylinder was the pressure required to react the pitch link load

$$PSI = \frac{PLL}{A_c} \tag{9}$$

where PLL is the pitch link load in lbs and A_C is the surface area of the working cylinder piston measured in in^2. PLL was directly measured from the axial strain gages on each actuator.

The flow rate was the volume of hydraulic fluid moved per minute as the cylinder area, A_C, was moved through its measured displacement stroke,

$$GPM = \left(\frac{dp}{dt} \cdot A_c\right) \cdot (0.004329) \tag{10}$$

where dp/dt is the velocity of the cylinder in units of in/min and 0.0004329 is the constant needed to convert in^3 to gallons. The units of time are minutes, not seconds.

Computation of the exact power per revolution was performed using the above formulas, taking care to represent the actuator PLL's and velocities as a time-varying quantities. Substituting Eqns. (9) and (10) into Eqn. (8) yields

$$HP = \frac{(PLL(t))\left(dp/dt\right) \cdot (A_c) \cdot (0.004329)}{(1714) \cdot (A_c)} \tag{11}$$

The quantities needed to size the hydraulic system are the maximum flow rate demanded by all four actuators at any one time and the instantaneous peak load experienced by the actuators. These quantities and the peak horsepower consumed by the actuators are presented in Table 6. The peak horsepower reported in Table 6 was not obtained using the maximum pitch link load and the maximum flow rate in the preceding columns because these do not necessarily occur at the same time, nor for all actuators at once. The peak IBC power for each actuator occurs when the product of its own pitch link load and its own flow rate is at a maximum. The peak horsepower was obtained by computing the instantaneous power consumed by each actuator using the time histories of the pitch link load and the position measurement signals. The peak power reported in Table 6 is the peak of the total instantaneous horsepower required by all four actuators at any time.

The actual power required from a ship power plant to operate a hydraulic pump is larger than the peak horsepower given in Table 6. This is where the ship supply pressure becomes important, because the greater the pressure to be supplied by the pump, the more ship horsepower required. The present IBC actuators used a working piston area of 0.657 in^2. Therefore, in order to react the highest pitch link load in Table 6, a hydraulic cylinder pressure of about 500 psi would be required. This means the hydraulic supply pressure would need to be about 2000 psi, assuming a 1000 psi drop across the servo-valves and a frictional line loss of 500 psi. The maximum flow rate indicated in Table 6 is about 20 GPM. As reported in Ref. 30, the power required to drive a pump at 20 GPM at 2000 psi is 27.5 HP, which is about half the power saved using 2/rev IBC at 170 kts (see Fig. 22). Nevertheless, the flow requirements for BVI noise and vibration suppression are only about 10 GPM, requiring about 14 ship HP to power the hydraulic pump. Therefore, at this point it seems most feasible to propose using IBC for noise and vibration suppression at low speed where the power required to drive the IBC actuators is low and a good amount of excess ship horsepower is available. Nevertheless, using IBC at high-speed did result in a net 2.5 percent power savings, which could grow larger at forward flight conditions having appreciable blade stall.

Table 6.
IBC Actuator Horsepower Requirements

Trim No.	IBC Input	Peak PLL lbs	Peak Flow GPM	Peak HP
2	2/rev, 1.5° at 60° phase	104	10.2	0.6
5	2/rev, 2.5° at 190° phase	332	16.5	3.1
1	2/rev, 2.5° at 60° phase	158	18.2	1.5
1	3/rev, 1.0° at 150° phase	199	7.6	0.8
2	3/rev, 1.0° at 135° phase	195	7.6	.7
2	6/rev, 0.5° at 135° phase	216	19.4	1.7
2	6/rev, 1.0° at 135° phase	139	9.7	.8

Conclusions

A full-scale wind tunnel test was conducted at the NASA Ames Research Center to evaluate the potential of helicopter individual blade control (IBC) to improve rotor performance, to reduce blade vortex interaction (BVI) noise, and to alleviate helicopter vibrations. The acquired data set indicated that up to 85 percent simultaneous reductions in both BVI noise and hub vibrations could be obtained using multi-harmonic IBC input. The data also showed that performance improvements of up to 7 percent could be obtained at the higher airspeeds.

Beyond any doubt, this investigation demonstrated the importance of using 2/rev IBC to reduce helicopter BVI noise, vibration, and power consumption. Because conventional HHC systems cannot correctly apply 2/rev control to four-(or more) bladed rotors, they cannot effectively be used to simultaneously suppress both BVI noise and vibration at the same time. Nevertheless, the other harmonic inputs are very important. It was remarkable that very small amplitudes of 3/rev, 4/rev, and 5/rev IBC (0.25 deg) were seen not only to very significantly enhance the noise and vibration reductions at low-speed, but also to be useful towards reducing cruise-speed vibrations as well.

The most significant findings of this research program are summarized as follows:

1) Applied separately, 2/rev IBC was very capable of suppressing both advancing and retreating side BVI noise levels using an amplitude of 1.5 deg at the 43 kt, 6 deg glide slope descent condition. Reductions in BVI noise up to a maximum of 10 db were obtained on the advancing side of the rotor while reducing the retreating side BVI noise by an average of 4 db at the same time. Moreover, the 4/rev hub loads were also reduced an average of 10 percent using this input.

2) The best simultaneous noise and hub load reductions were obtained by using a combination of 1.5 deg of 2/rev IBC with 0.25 deg 5/rev IBC. This input was able to suppress the total 4/rev hub vibrations by 85 percent while simultaneously reducing the peak advancing side BVI noise up to a maximum of 12 db and the retreating side BVI noise up to 4 db at the same time. Although increasing the 5/rev input to 1.0 deg nearly doubled the 4/rev vibration, it provided an average retreating side BVI noise suppression of 12 db, while still reducing the average advancing side BVI noise by an average 6 db.

3) Simultaneous reduction of advancing side BVI noise, retreating side BVI noise, and 4/rev hub vibration was not possible using 3/rev, 4/rev, or 5/rev IBC applied alone or in combination with each other. For these harmonics, the phase angles producing the best vibration reductions are different from those required for optimal BVI noise suppression.

4) In the low-speed transition region ($\mu = 0.1$), 2/rev, 3/rev, and 4/rev IBC, applied separately, were seen to significantly reduce the predominant 4/rev vibratory hub forces and moments. Whereas up to 80 percent simultaneous suppression of the in-plane hub forces and moments could be obtained using 2.5 deg of 2/rev IBC, up to 99 percent of the 4/rev vertical shear forces could be suppressed using 1.0 deg of 3/rev IBC.

5) Vibration suppression at high-speed ($\mu = 0.3$) may be obtained using 3/rev and 4/rev IBC input amplitudes significantly less than one deg. It is doubtful that 2/rev IBC can be used to effectively control vibration at high-speed because of its tendency to disturb the hub moment trim equilibrium.

6) With few exceptions, the vibratory hub moments and in-plane shear forces tended to be decreased (or increased) together as the IBC inputs were varied in phase and amplitude. This implies a reduction in the number of vibration degrees of freedom from five to two (lift + 1 other) might be possible, thereby potentially simplifying controller development when using a hub load measuring device by reducing the measurement state vector.

7) Significant total rotor power reductions of up to 7 percent were obtained using 2/rev IBC at advance ratios higher than $\mu = 0.3$ (127 kts). The introduction of 2/rev IBC at $\mu = 0.40$ to 0.45 did not increase the rotor blade bending and pitch-link loads (IBC actuator axial load) at the phase angles of best power reduction. This allows room for further power reductions using control authorities higher than 2.5 deg.

8) At low speeds, IBC increased the pitch link loads and blade bending loads significantly. Although the 2/rev IBC increased the pitch link and blade torsional loads the least, it also increased the blade flapwise and chordwise bending moments the most. However, at high-speed forward-flight conditions, the 2/rev inputs did not significantly effect the pitch link or blade bending loads.

9) Although the power consumed by the IBC actuators was found to be very small (1-3 HP), the ship horsepower required to supply the hydraulic flow was considerably larger (14-28 HP). Therefore, at this point it seems most feasible to propose using IBC for noise and vibration suppression at low speed where the power required to drive the IBC actuators is low and a good amount of excess ship horsepower is available. Nevertheless, using IBC at high-speed did result in a net 2.5 percent power savings, which could grow larger at forward flight conditions having appreciable blade stall.

Acknowledgments

This international research program was made possible only by the cooperation of many individuals at Ames Research Center and throughout Germany. The authors wish to thank Mr. Karl-Heinz Bock, Mr. Hans-Jurgen Goette, Mr. Thomas Schreiber, and Mr. Michael Platzer of ZF Luftfahrttechnik GmbH for their extraordinary efforts made preparing, installing, and operating the IBC system. Many thanks also go to Mr. Stephen Swanson (Sterling Software at Ames) for his help acquiring and analyzing the acoustic data. The coordination efforts under the MOU of Dr. Peter Hamel (DLR), Mr. Bernd Gmelin (DLR), Mr. Dave Key (U.S. Army), Mr. Andrew Kerr (U.S. Army), Dr. William Warmbrodt (NASA Ames), Mr. Peter Richter (ZF Luftfahrttechnik), and Dr. Dieter Braun (Eurocopter Deutschland) are also gratefully acknowledged.

References

1) Stewart, W., "Second Harmonic Control on the Helicopter Rotor", Aeronautical Research Council, Reports and Memoranda Number 2997, August, 1952.

2) Arcidiacono, P. J., "Theoretical Performance of Helicopters having Second and Higher Harmonic Feathering Control," Journal of the American Helicopter Society, Vol. 6, No. 2, April 1961.

3) Drees, J. M., and Wernicke, R. K., "An Experimental Investigation of a Second Harmonic Feathering Device on the UH-1A Helicopter," U.S. Army Transportation Research Command, TR-62-109, Fort Eustis, Virginia, June 1963.

4) McCloud, J.L., III, and Kretz, M., "Multicyclic Jet-Flap Control for Alleviation of Helicopter Blade Stresses and Fuselage Vibration", NASA SP-352, 1974.

5) Ham, N.D., "Helicopter Individual-Blade Control and its Applications", 39th Annual Forum of the American Helicopter Society, St. Louis, MO, May 1983.

6) Kretz, M., "Active Expansion of Helicopter Flight Envelope",15th European Rotorcraft Forum, Amsterdam, The Netherlands, September 1989.

7) Hammond, C.E., "Wind Tunnel Results Showing Rotor Vibratory Loads Reduction Using Higher Harmonic Blade Pitch", Journal of the American Helicopter Society, Vol. 28, No. 1, Jan. 1983.

8) Wood, E.R., Powers, R.W., Cline, J.H., and Hammond, C.E., "On Developing and Flight Testing a Higher Harmonic Control System", Journal of the American Helicopter Society, Vol. 30, No. 1, January 1985.

9) Gupta, B.P., Wood, E.R., Logan, A.H., and Cline, J.H., "Recent Higher Harmonic Control Development and OH-6A Flight Testing", 41st Annual Forum of the American Helicopter Society, Fort Worth, TX, May 1985.

10) Shaw, J., Albion, N., Hanker, E.J., and Teal, R.S., "Higher Harmonic Control: Wind Tunnel Demonstration of Fully Effective Vibratory Hub Force Suppression", 41st Annual Forum of the American Helicopter Society, Fort Worth, TX, May 1985.

11) Straub, F. and Byrns, E., "Application of Higher Harmonic Blade Feathering on the OH-6A Helicopter for Vibration Reduction", NASA CR 4031, 1986.

12) Polychroniadis, M., and Achache, M. "Higher Harmonic Control: Flight Tests of an Experimental System on SA 349 Research Gazelle", 42nd American Helicopter Society Forum, Washington, D.C., June 1986.

13) Miao, W., Kottapalli, S.B.R., and Frye, M. M., "Flight Demonstration of Higher Harmonic Control (HHC) on S-76", 42nd Annual Forum of the American Helicopter Society, Washington, D.C., June 1986.

14) Kube, R., "Evaluation of a Constant Feedback Gain for Closed Loop Higher Harmonic Control", 16th European Rotorcraft Forum, Glasgow, Scotland, September 1990.

15) Kube, R., Achache, M., Niesl, G., and Splettstoesser, W. "A Closed-loop Controller for BVI Noise Reduction by Higher Harmonic Control", 48th Annual Forum of the American Helicopter Society, Washington, D.C., June 1992.

16) Splettstoesser, W.R., Schultz, K.-J., Kube, R., Brooks, T.F., Booth Jr., E.R., Niesl, G., and Streby, O., "A Higher Harmonic Control Test in the DNW to Reduce Impulsive BVI Noise", Journal of the American Helicopter Society, Vol. 39, No. 4, October 1994.

17) Yu, Y.H., Gmelin, B., Heller, H., Philippe, J.J., Mercker, E., and Preisser, J.S., "HHC Aeroacoustics Rotor Test at the DNW - The Joint German/French/US HART Project", 12th European Rotorcraft Forum, Amsterdam, The Netherlands, October 1994.

18) Millott, T., and Friedmann, P., "Vibration Reduction in Hingeless Rotors Using an Actively Controlled Trailing Edge Flap: Implementation and Time Domain Simulation", 35th AIAA/ASME/ASCE Structures, Structural Dynamics, and Materials Conference, Hilton Head, SC, April 1994.

19) Richter, P., Eisbrecher, M.-D, and Kloppel, V., "Design and First Flight Test of Individual Blade Control Actuators", 16th European Rotorcraft Forum, Glasgow, Scotland, September 1990.

20) Teves, D., Kloppel, V., and Richter, P., "Development of Active Control Technologies in the Rotating System, Flight Testing and Theoretical Investigations", 18th European Rotorcraft Forum, Avignon, France, September 1992.

21) Jacklin, S. A., Leyland, J. L., and Blaas, A., "Full-Scale Wind Tunnel Investigation of a Helicopter Individual Blade Control System", 34th AIAA/ASME/ASCE Structures, Structural Dynamics, and Materials Conference, La Jolla, CA, April 1993.

22) Richter, P. and Blaas, A, "Full-Scale Wind Tunnel Investigation of an Individual Blade Control System for the BO-105 Hingeless Rotor", 19th European Rotorcraft Forum, Como, Italy, September 1993.

23) Jacklin, S.A., Nguyen, K.Q., Blaas, A., and Richter, P., "Full-Scale Wind Tunnel Test of a Helicopter Individual Blade Control System", 50th Annual Forum of the American Helicopter Society, Washington, D.C., May 1994.

24) Swanson, S.M., Jacklin, S.A., Blaas, A., Kube, R., Niesl, G., "Individual Blade Control Effects on Blade-Vortex Interaction Noise", 50th Annual Forum of the American Helicopter Society, Washington, D.C., May 1994.

25) Jacklin, S.A., Blaas, A., Teves, D., and Kube, R., "Reduction of Helicopter BVI Noise, Vibration, and Power Consumption Through Individual Blade Control", 51th Annual Forum of the American Helicopter Society, Fort Worth, TX, May 1995.

26) Swanson, S.M., Jacklin, S.A., Blaas, A., Niesl, G., and Kube, R., "Acoustic Results from a Full-Scale Wind Tunnel Test Evaluating Individual Blade Control", 51th Annual Forum of the American Helicopter Society, Fort Worth, TX, May 1995.

27) Johnson, W., Helicopter Theory, Princeton University Press, New Jersey, pp. 694-698, 1980.

28) Vuilet, A., "The High-Speed Helicopter", 18th European Rotorcraft Forum, Avignon, France, September 1992.

29) Johnson, W., "Development of a Comprehensive Analysis for Rotorcraft I, II", *Vertica*, Vol. 5, pp. 99-129 and pp. 185-216, 1981.

30) NTT, Fluid Power Data Book,Womack Educational Publications, Dallas, TX, p 32, 1994.